Wetting in Color: Colorimetric Differentiation of Organic Liquids with High Selectivity

Ian B. Burgess,[†,*] Natalie Koay,[‡,§,∥] Kevin P. Raymond,[‡,§,∥] Mathias Kolle,[†] Marko Lončar,[†] and Joanna Aizenberg[†,‡,⊥,*]

[†]School of Engineering and Applied Sciences and [‡]Wyss Institute for Biologically Inspired Engineering, Harvard University, Cambridge, Massachusetts 02138, United States, [§]University of Waterloo, Waterloo, Canada N2L 3G1, and [⊥]Department of Chemistry and Chemical Biology, Harvard University, Cambridge, Massachusetts 02138, United States [∥]These authors contributed equally to this work.

ABSTRACT Colorimetric litmus tests such as pH paper have enjoyed wide commercial success due to their inexpensive production and exceptional ease of use. Expansion of colorimetry to new sensing paradigms is challenging because macroscopic color changes are seldom coupled to arbitrary differences in the physical/chemical properties of a system. Here we present in detail the design of a "Wetting In Color Kit" (WICK), an inexpensive and highly selective colorimetric indicator for organic liquids that exploits chemically encoded inverse-opal photonic crystals to project minute differences in liquids' wettability to macroscopically distinct, easy-to-visualize structural color patterns. We show experimentally and corroborate with theoretical modeling using percolation theory that the highly symmetric structure of our large-area, defect-free SiO_2 inverse-opal films leads to sharply defined threshold wettability for liquid infiltration, occurring at intrinsic contact angles near 20° with an estimated resolution smaller than 5°. The regular structure also produces a bright iridescent color, which disappears when infiltrated with liquid, naturally coupling the optical and fluidic responses. To deterministically design a WICK that differentiates a broad range of liquids, we introduced a nondestructive quality control procedure to regulate the pore structure and developed two new surface modification protocols, both requiring only silanization and selective oxidation. The resulting tunable, built-in horizontal and vertical chemistry gradients let us tailor the wettability threshold to specific liquids across a continuous range. With patterned oxidation as a final step, we control the shape of the liquid-specific patterns displayed, making WICK easier to read. Using these techniques, we demonstrate the applicability of WICKs in several exemplary systems that colorimetrically distinguish (i) ethanol—water mixtures varying by only 2.5% in concentration; (ii) methanol, ethanol, and isopropyl alcohol; (iii) hexane, heptane, octane, nonane, and decane; and (iv) samples of gasoline (regular unleaded) and diesel. As wetting is a generic fluidic phenomenon, we envision that WICK could be suitable for applications in authentication or identification of unknown liquids across a broad range of industries.

KEYWORDS: photonic crystals · wetting · colorimetric sensing · inverse-opals · surface chemistry · encryption

Structural color, derived from coherent scattering from wavelength-scale roughness or porosity, has received considerable interest in the development of new technologies, largely due to its broad capacity for tuning.[1−18] In particular, the prospect of easy-to-read, self-reporting sensors, which are based on structural color changes induced by specific chemical or physical properties of an unknown, has the promise to greatly expand the availability of portable and inexpensive diagnostics beyond those amenable to specific chemical processes or complex optical readouts.[19−29] Structural color is tied to a wide range of changes in the *physical* properties of a material forming the structure (*e.g.*, the shape and density of a material) rather than a specific *chemical* state responsible for absorption in a characteristic wavelength region (*e.g.*, a protonated or deprotonated molecule in pH indicators). This color, therefore, has no inherent specific chemical requirements (*e.g.*, any material with periodic roughness displays iridescence as long as the periodicity is comparable to the wavelengths of visible light).[19−29] This gives immense flexibility in the chemical properties of structural colorimetric sensors. Thus, tunable structural color carries the potential for broad applicability in colorimetric sensing. With chemistry as a versatile degree of freedom, structured materials have been engineered to change their shape, volume, or density and thus their color in response to pH,[23,24,26] magnetic fields,[17] vapor adsorption,[19,20,28] and mechanical strain[12,25] to name a few.[5]

To design a sensitive, self-reporting colorimetric indicator that can be used over a broad class of materials would require (1) the ability to encode multiple responses, and thus complex chemical information into a single material;[7,30−40] (2) high sensitivity to a general property defined for a wide class of materials (*i.e.*, mass, density, surface tension, *etc.*);[41,46] and (3) an easy to detect colorimetric response.

Recently, we demonstrated that defect-free silica inverse-opal films (IOFs)[42] can be encoded to display distinct wetting patterns in different liquids by functionalizing them with a spatial pattern of organic surface groups.[43] These patterns are clearly visible

* Address correspondence to ibburges@fas.harvard.edu, jaiz@seas.harvard.edu.

Received for review November 1, 2011 and accepted December 20, 2011.

Published online December 20, 2011
10.1021/nn204220c

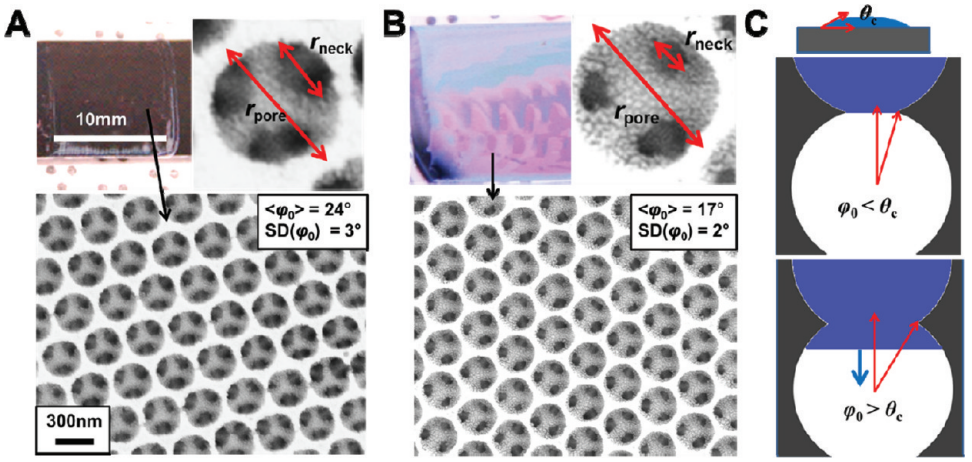

Figure 1. (A,B) Optical images of IOFs uniformly functionalized with DEC groups, submerged in 85% ethanol (aq) (top) and corresponding representative SEM images of the pore structure (bottom). Although the surface chemistry is the same in both cases, different wetting outcomes are observed in the same liquid due to the larger relative size of the interpore necks in the sample shown in (A). (C) Schematic illustrating the relationship between the neck angle (φ_0, where $\sin(\varphi_0) = r_{neck}/r_{pore}$) and the wetting response. Infiltration of a pore occurs if the intrinsic contact angle (θ_c, where $\cos(\theta_c) = [\gamma_{sa} - \gamma_{sl}]/\gamma_{la}$) is less than φ_0 (bottom schematic), while no infiltration occurs for smaller pores where $\varphi_0 < \theta_c$ (top schematic).

due to the large difference in refractive-index contrast between the wetted and nonwetted regions of the 3D photonic crystal. We used this concept to demonstrate a platform for multilevel encryption that we called W-Ink.[43] The W-Ink encryption platform has the potential to satisfy all three of the above requirements for a colorimetric indicator for liquids. As we show here, it allows for different liquids to produce distinct color patterns according to wettability, a universal property.

This paper presents a thorough analysis of this highly selective wetting phenomenon observed in IOFs and demonstrates how it can be manipulated through simple and robust techniques to tune the surface chemistry. We show that the remarkable selectivity of wetting is caused by the unique, highly symmetric pore geometry of IOFs fabricated by colloidal co-assembly.[42] The selectivity is found to be a function of the uniformity of the sizes of the IOFs' interpore openings. Using percolation modeling to corroborate our wetting experiments and structural analysis of the IOFs, we determine that the colorimetric response is selective to differences in intrinsic contact angle ($\cos(\theta_c) = [\gamma_{sa} - \gamma_{sl}]/\gamma_{la}$, where γ_{sa} is the solid−air surface tension, *etc.*) smaller than 5° when the surface chemistry is spatially uniform. This selectivity can be increased when the surface chemistry is graded vertically. We show that this selectivity is ultimately limited by short-range disorder in the pore geometry.

Using these insights, we demonstrate how the W-Ink concept can be expanded to develop a "Wetting In Color Kit" (WICK)—an indicator that displays distinct colorimetric patterns in liquids in response to subtle differences in their wettability. As the colorimetric selectivity only exists at a specific wettability threshold (intrinsic contact angle, $\theta_c \sim 20°$), a WICK displaying mutually distinct colorimetric responses in n different liquids requires spatial regions containing at least $n - 1$ different surface functionalities. Furthermore, the ability to practically exploit WICK for liquid *identification* requires that IOFs have access to a continuously adjustable range of surface functionalities. This allows for specific colorimetric responses to be designed to distinguish specific liquids that are designated *a priori*. To address these challenges, we describe two protocols in this paper based on chlorosilane chemistry and plasma oxidation, which give us the power to generate continuously adjustable surface chemistry within the pores. We also implement a nondestructive quality control procedure to regulate the pore geometry. These protocols allow us to both maximize the selectivity of the indicator and give us the capability to design a WICK that mutually colorimetrically differentiates arbitrary sets of liquids. We present several examples to illustrate this point: differentiating between water dilutions of ethanol with selectivity down to 2.5% differences in concentration; differentiating different pure alcohols (methanol, ethanol, isopropyl alcohol), and alkanes (hexane, heptane, octane, nonane, decane); and differentiating between different grades of automotive fuel (gasoline and diesel).

RESULTS AND DISCUSSION

Determining the Selectivity Limits. *Correlation between Pore Structure and Wetting.* Our IOFs each consist of a SiO_2 slab with a regular array of spherical air pores arranged in a face-centered cubic (fcc) lattice.[42] Nearest neighbors are connected by small openings (necks). Scanning electron microscope (SEM) images of two IOFs are shown in Figure 1A,B. When a porous material is immersed in liquid, spontaneous filling of the pores

requires both an energetically favorable liquid–solid interaction (*i.e.*, $\theta_c < 90°$) and the absence of an activation barrier (metastable state) associated with the propagation of the fluid front through the structure.[44] When a liquid front propagates through the narrow interpore necks, there is a free-energy trade-off between the favorable wetting of the solid surface (assuming $\theta_c < 90°$) and the unfavorable creation of a liquid–air interface.[43,44] An activation barrier associated with the propagation of the liquid front through the neck exists if θ_c is larger than the azimuthal angle subtended by the narrow neck between the pores[43] (shown schematically in Figure 1C). For a given liquid and pore surface functionality, the corresponding θ_c defines a critical neck angle, smaller than which the liquid front will not be able to pass from one pore to the next.

Therefore, the ability to precisely control the infiltration of liquids (and thus the colorimetric response to liquids) relies on our ability to control two parameters: (i) the surface chemistry (which determines θ_c) and (ii) the IOF's neck angles (which determine the critical θ_c for infiltration). In this paper, surface chemistry is treated as a tuning parameter, which we exploit to illustrate highly liquid-selective control of wetting. However, this selectivity is ultimately limited by our ability to regulate the pore structure.

In a perfectly symmetric IOF with exactly identical neck widths throughout, the transition between an IOF that is completely impervious to liquid infiltration (displaying iridescent color) and one that is fully infiltrated (transparent, showing the color of the underlying substrate) at equilibrium would occur over an infinitesimally narrow range of liquid contact angles (θ_c). Given a technique to specify the surface chemistry of the pores with unlimited adjustability and precision, we could design a colorimetric indicator based on such a "perfect" structure that could detect arbitrarily small differences in wettability. A critical requirement for the practical realization of a sensitive colorimetric indicator is to be as close as possible to this "perfect" theoretical structure. An inherent advantage of using IOFs fabricated by colloidal co-assembly for these studies is that they are characterized by an exceptionally regular structure.[42] However, they do display some degree of both short-range (<mm scale) and long-range (>mm scale) variations in the neck angles (φ_0). These variations must be considered to understand the wetting response and controlled for as much as possible if we are to reproducibly study the effects of surface chemistry.

Figure 1A,B illustrates the effects of sample-to-sample variability in φ_0 on the wetting outcomes when the surface chemistry is fixed. The samples are functionalized with *n*-decylsilyl (DEC) groups (from exposure to vapors of the corresponding alkylchlorosilane).[43] Photographs (top) show the two IOFs immersed in

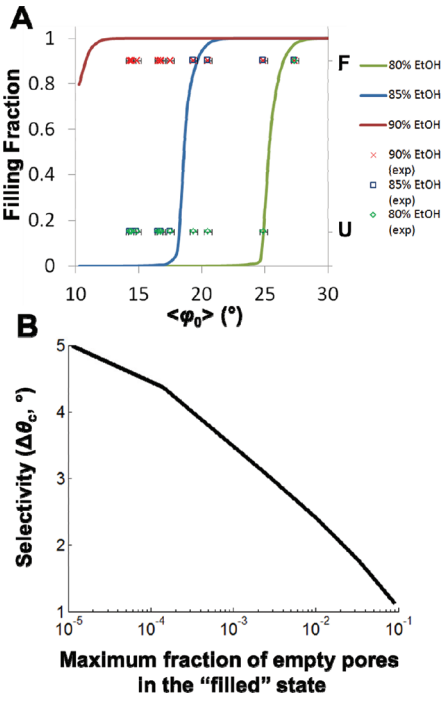

Figure 2. (A) Simulated equilibrium filling percentages calculated from the neck angle (φ_0) distribution using percolation modeling of IOFs functionalized uniformly with DEC groups immersed in 80, 85, and 90% ethanol (aq). Isolated points overlaid correspond to mean neck angles ($\langle\varphi_0\rangle$) measured from SEM images. The *y*-axis values (right axis) depict the colorimetric state observed (F = filled, U = unfilled) in 80% EtOH (green diamonds), 85% EtOH (blue squares), 90% EtOH (red X's). (B) Predicted selectivity limits (expressed in terms of θ_c) as a function of the maximum tolerated fraction of unfilled pores defined as the filled state. The colorimetric unfilled state is defined as having bond connectivity below the percolation threshold for an fcc lattice (12%). Limits are calculated assuming a maximum short-range neck angle standard deviation of 3.2°, determined experimentally.

85 vol % ethanol (EtOH) in water. The film in Figure 1A is infiltrated by the liquid (discernible from the disappearance of color), while the film in Figure 1B is not infiltrated (bright iridescent color remains). As shown in the SEM images (bottom), the more easily infiltrated IOF is characterized by larger φ_0. We estimated the neck angles by measuring the ratio of the pore and neck widths (measured in the tangential direction), using $\sin(\varphi_0) = r_{neck}/r_{pore}$.

This estimation relies on the assumptions that our pores are near-spherical and that the top layer (where the neck widths can be easily measured) represents well the structure throughout. As φ_0 is derived from a ratio of lengths, scaling errors (*e.g.*, calibration) in the SEM imaging do not affect our estimation. The mean and standard deviation in neck angles measured from the images shown in Figure 1A,B are indicated on the images. The maximum short-range standard deviation in the neck angles estimated from the largest value for short-range variability measured from a single SEM image was 3.2°. This estimated upper-bound value was

further used in theoretical study that projected the selectivity limits described below.

Theoretical Selectivity Limit (Uniform Surface Chemistry). Using intrinsic contact angles measured from DEC-functionalized flat surfaces,[43] we derived the expected equilibrium filling states from bond connectivities using a numerical percolation simulation. The model considered an fcc lattice of pores, 30 close-packed layers thick, with a large lateral area (10^4 unit cells). Neck angles were randomly assigned to each nearest-neighbor connection according to a normal distribution. Inputting θ_c and starting with a completely filled top layer (as these are half-spheres in our IOFs and have no re-entrant curvature,[42] see SEMs and schematics in Figure 1), the simulation filled all pores with paths of interpore fluid connectivity (*i.e.*, where $\varphi_0 > \theta_c$) connecting them to the top filled layer. The solid curves in Figure 2A show the simulated overall filling fraction for 90% ($\theta_c = 13 \pm 5°$), 85% ($\theta_c = 22 \pm 5°$), and 80% ($\theta_c = 29 \pm 5°$) EtOH for DEC-functionalized IOFs as a function of mean neck angle. A standard deviation of 3° was used in these simulations (Figure 2A).

To verify the correlation between the neck angle and the wetting behavior, we characterized the neck angle distribution (from SEM images sampled randomly across each film) and the infiltration state (from the presence or absence of iridescent color) in 80, 85, and 90% EtOH of 12 IOFs uniformly functionalized with DEC groups. These measurements are represented by the isolated points in Figure 2A. Figure 2A shows good agreement between our theoretical predictions and experimental results, confirming that the long-range variation in the response of a DEC-functionalized IOF to these liquids correlates to the long-range variation in the neck angles. As described in the next section, we can exploit this to develop a nondestructive quality control procedure to limit the effect of long-range variability in the neck angles.

Short-range variability in the neck angles is what ultimately limits the selectivity of an IOF's colorimetric response to liquids. Infiltration of a liquid through an IOF with uniform surface chemistry and a random distribution of neck angles will proceed as percolation through a regular fcc lattice[45] with a bond connectivity determined by θ_c. The final equilibrated infiltration state will be a statistical distribution of filled and empty pores over a range of θ_c determined by the local variance of φ_0. To extract a colorimetric selectivity from this continuous distribution of partial filling states, we must determine what constitutes "easily visually distinct" color patterns, which is inherently subjective. In this paper, we choose to define easily visually distinct patterns as those with countable differences (*e.g.*, each region can only be assigned two possible states). Therefore, we assume a user can only designate a region with uniform surface chemistry as being "unfilled" (bright color) and "filled" (transparent, negligible contrast with the underlying substrate).

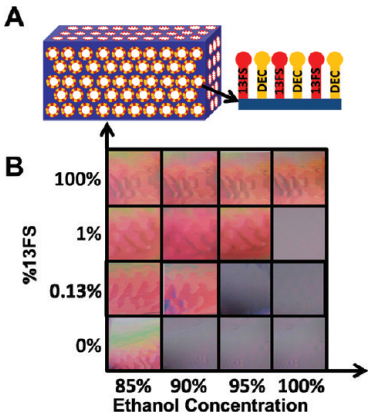

Figure 3. (A) Schematic depicting the formation of mixed monolayers by evaporating mixtures of two alkylchlorosilanes (13FS in red and DEC in yellow) to produce wetting responses that span the range between that of a homogeneous monolayer of each. (B) Colormap illustrating an array of IOFs (each square is 1 cm × 1 cm), functionalized with various mixed monolayers of 13FS and DEC, that allow mutual colorimetric distinction of 85, 90, 95, and 100% ethanol (aq). All photographs in a single row are of the same IOF. The *y*-axis denotes the volume fraction of 13FS-trichlorosilane used in the liquid−liquid mixture that evaporated onto the IOF.

We choose a maximum fraction of filled pores that defines the colorimetric unfilled state and a maximum fraction of unfilled pores that defines the filled state. In this definition, the colorimetric selectivity (minimum resolvable difference in θ_c) is defined by the range of θ_c over which the filling fraction does not fit into either of these definitions. To extract this range, we choose lower and upper bounds of connectivity to define the resolution limit of our colorimetric indicator. In our estimation of the colorimetric selectivity, we chose the bond percolation threshold that occurs at 12% connectivity for an fcc lattice[45] as the upper-bound connectivity defining the unfilled state. For connectivity below this bond percolation threshold, all paths of fluid flow have finite length.[45] This means that a sufficiently thick IOF will have completely empty layers at equilibrium, thereby producing color that can be easily distinguished from the filled state.

We define the onset of the filled state by a maximum tolerance of empty pores. Figure 2B plots the selectivity (expressed in terms of θ_c) as a function of this tolerance. The smallest tolerance shown in Figure 2B (1 unfilled pore per 10^5 unit cells) should be a conservative estimate of this limit. The 10^5 unit cells per unfilled pore corresponds to an average distance of >30 μm (>100 unit cells) between scattering centers and a fractional scattering cross-sectional area of $<10^{-4}$ for a film of typical thickness of 5 layers illuminated from above. Thus the scattered intensity from empty pores will be very low in this limit (the film appears transparent). Therefore, an IOF with uniform

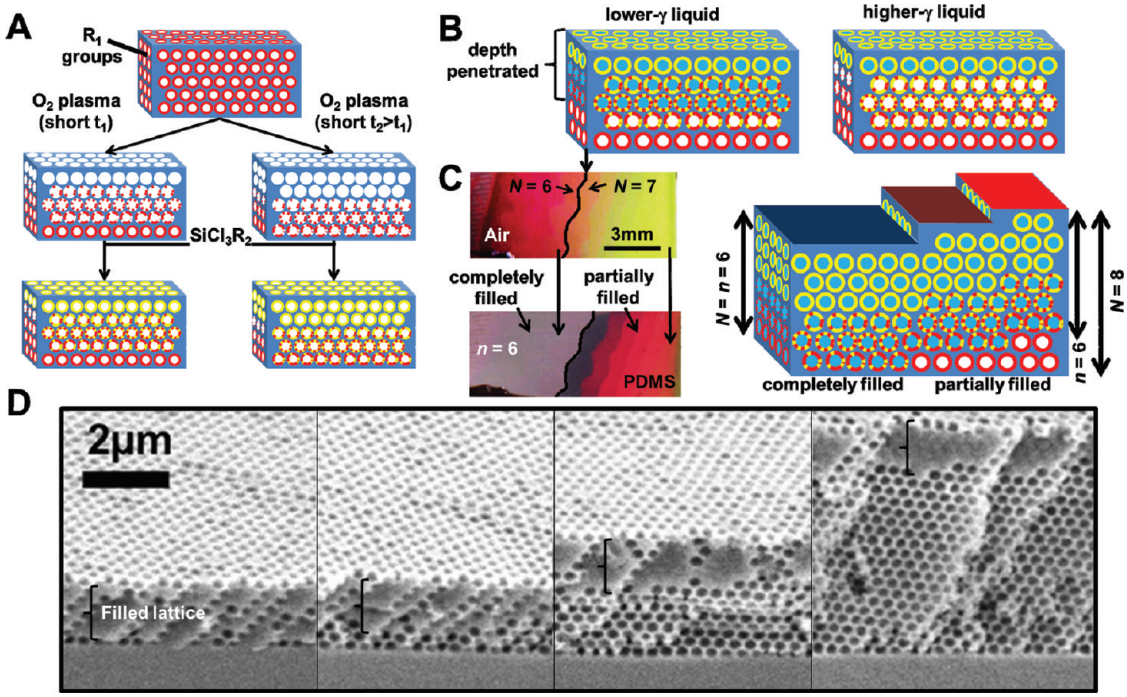

Figure 4. (A) Schematic depicting the use of short O_2 plasma exposure between successive silanizations to generate a vertical gradient of wettability. (B) Using vertical gradients where wettability decreases toward the bottom of the sample, liquids penetrate up to a fixed depth that increases with decreasing surface tension (decreasing θ_c). The blue circles represent pores that are filled with liquid in the schematics. (C) This depth translates into a distinct color pattern in IOFs having a naturally varying total number of layers (shown in schematic). Photographs show an IOF-functionalized DEC→13FS (45 s plasma exposure) in air (top) and after soaking in PDMS precursors (cured before imaging). The total thickness of this IOF is increasing from the left to the right of the image. The color completely disappears in the regions where the total thickness is less than the penetration depth ($n = 6$). The black line on the images indicates the boundary between regions with 6 and 7 total layers (N). (D) Scanning electron micrograph (SEM) cross-sections illustrating the fixed degree of layer penetration of the PDMS precursors (subsequently cured) over a wide range of film thicknesses.

surface chemistry has the capacity to colorimetrically differentiate liquids based on differences in θ_c of less than 5°. This corresponds to concentration selectivity of at least 5% in water–ethanol mixtures.[43]

Design and Optimization of WICK. *Structural Quality Control.* Figure 2A shows that the variability in the surface chemistry (at least for DEC functionality) is generally below that of the neck angles. However, it also illustrates that while the short-range variability of the IOF neck angles is generally small (SD ≤ ~3°) the variability from one sample to the next can be sufficiently large to skew the effects of surface chemistry. To limit this effect, we introduced a quality control step in the studies described below: All samples described hereafter were first uniformly functionalized with DEC groups and characterized optically in 85 and 90% EtOH. In order to be considered for further use, the IOF must display an unfilled state (no loss of iridescent color) in 85% EtOH and a filled state (no contrast with the blank substrate) in 90% EtOH (see bottom row of Figure 3B for example). Satisfying this requirement means that the neck sizes are in the range for which precise colorimetric response can be controlled by surface chemistry. After a sample passes this test, the DEC functionality is removed by oxygen plasma and subsequent acid piranha cleaning, and the samples are refunctionalized in one of the manners described below. This limits the mean neck angles to approximately the range of 14–18° (see Figure 2A). Consistent with the statistics displayed in Figure 2A, roughly one-third of the samples prepared using the co-assembly method[42] showed out-of-range neck angles and were discarded as a result of this quality control process.

Generating Continuously Adjustable Wettability. To use WICK to differentiate any two liquids, it is essential to be able to encode a continuous range of wettability in the IOFs. In contrast to the encryption-type application of the W-Ink platform described previously[43] (where the decoding solvents can be determined *a posteriori* based on the availability of specific alkylchlorosilanes), effective design of a solvent *indicator* requires that one can choose two liquids for differentiation *a priori* and then be able to tune the surface chemistry such that the IOF displays different filling states in each liquid. We have developed two different techniques for tailoring surface functionality continuously. In both approaches, one requires only two alkylchlorosilanes, $SiCl_3R_1$ and $SiCl_3R_2$, where the IOF functionalized with only the R_1 groups displays the unfilled state and the IOF functionalized with the R_2 groups displays the filled state in both liquids. To illustrate these techniques, we used 13FS (1*H*,1*H*,2*H*,2*H*-tridecafluorooctyl)silyl and DEC groups as

R_1 and R_2 and ethanol–water mixtures of varying concentration to produce a continuum of surface tensions (and values of θ_c). 13FS-functionalized IOFs display an unfilled state in all water–ethanol mixtures (including 100% EtOH), and DEC-functionalized IOFs display a filled state in EtOH concentrations larger than 85% (as enforced by quality control). In the "Guiding the Eye" section, we illustrate the general applicability of these techniques, performing analogous optimizations, but replacing water–ethanol mixtures with several other classes of liquids (pure alcohols, pure alkanes, different auto fuels).

Perhaps the most intuitive method to functionalize an IOF such that the wettability displayed lies between that from homogeneous coatings of 13FS and DEC is to deposit a mixture of 13FS and DEC groups on the surface (illustrated in Figure 3A). We generated mixed 13FS:DEC monolayers by exposing IOFs to vapors from a mixture of 13FS- and DEC-trichlorosilanes. Adjusting the relative concentration of 13FS- and DEC-trichlorosilanes in the liquid–liquid mixture should alter the relative density of groups on the surface and was used to tune the infiltration threshold to occur at any ethanol concentration between 85 and 100%. Figure 3B is a response colormap showing four samples (each row is one IOF) functionalized with 13FS, DEC, and different mixtures of the two. Using mixtures of 13FS and DEC groups, we were able to create IOFs whose wetting threshold occurs at 90 and 95% EtOH. By comparing the columns of the colormap, we see that samples with these four functionalities produce an array that colorimetrically identifies the relative concentration of a water–ethanol mixture to a precision of 5% across the full range selectivity offered by DEC and 13FS functionalities (85–100% EtOH).

Vertical Gradients of Wettability. Generating continuous gradients of wettability in an IOF is a second method that can be used to produce distinct color imetric responses across a continuous range of surface tensions. We generated vertical gradients of wettability using *short* plasma exposure times (insufficient to completely remove the existing groups throughout the depth of the structure) between successive silane depositions.[35,43] Lin *et al.*[35] showed that oxygen plasma propagates through tightly confined channels slowly (several minutes for 20 μm wide channels) and results in a graded surface chemistry near the front. Depicted in Figure 4A, we first functionalized an IOF with the more lyophobic group (R_1, 13FS). Following a short (<2 min) exposure of the structure to oxygen plasma, we expect incomplete removal of the R_1 groups, with the efficiency of removal decreasing with increasing depth. Subsequent addition of less lyophobic groups (R_2, DEC) *via* exposure to $SiCl_3R_2$ vapors generates a mixed, graded surface chemistry with an increasing ratio of R_2/R_1 from the bottom to the top of the IOF.

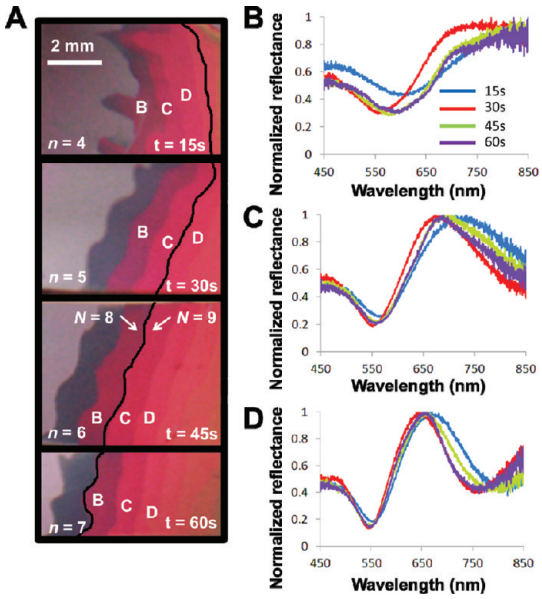

Figure 5. (A) Photographs of four segments of an IOF functionalized with a DEC→13FS vertical gradient using different plasma exposure times, from top: 15, 30, 45, and 60 s, submerged in PDMS precursors. The number of completely filled layers (*n*) is listed on each image (verified by SEM after curing). The black line drawn on the images indicates the boundary between regions with 8 and 9 total layers (*N*). (B–D) Normalized reflectance spectra for the three colored stripes indicated in (A) showing that the color is sensitive to neither *N* nor *n* independently, but depends only on ($N - n$).

We expect IOFs with vertical gradients of chemistry (in which the wettability decreases with depth) to display distinct partial infiltration patterns in incrementally different liquids, each penetrating a fixed depth (Figure 4B). As the total thickness of our IOFs can be made to gradually vary across the sample (naturally occurring in vertical evaporative depositions),[42] distinct depths of penetration are viewed as distinct rainbow patterns whose size and location in the chip is unique to the depth filled. The schematic in Figure 4C illustrates this principle. The top photo in Figure 4C shows a film that has been functionalized uniformly with 13FS groups, exposed to oxygen plasma for 45 s, and then functionalized with DEC groups. The total thickness of the film varies from only two close-packed layers on the far left to a large number (>20 layers) on the far right, each visible "stripe" representing a region of fixed thickness, having one more layer than the stripe to the left of it. In thinner regions ($N < \sim 10$), these stripes are wide enough to be visible by eye (~0.5–1 mm wide). In the thickest regions, very close to the edges, the thickness increases on shorter length scales and the stripes become harder to resolve. To characterize the differences in the liquid infiltration that can be achievable with such a vertical gradient, we immersed the IOF in liquid precursors to polydimethylsiloxane (PDMS, Sylgard 184). The sample was subsequently cured to allow visualization of the filled layers by SEM.

Figure 4C shows that the liquid completely penetrates the first 6 layers ($n = 6$), and the IOF becomes transparent (displaying the gray of the silicon substrate) in regions where the total number of layers is $N \leq 6$. SEM cross sections in Figure 4D show the consistent penetration depth from the top of the IOF that is independent of the total thickness.

The color displayed by an IOF having N layers, the top n of which are filled ($n < N$), should match the color produced by an empty ($N - n$) layer IOF. This is because the filled regions become transparent, provided there is sufficient refractive index matching between the fluid and the silica (this is true, for example, when the precursors to PDMS is the liquid used). Figure 5A shows four segments of an IOF, all functionalized with a DEC→13FS vertical gradient using different plasma exposure times and immersed in PDMS precursors (subsequently cured). Owing to the varied oxygen plasma exposure time, the PDMS completely filled the lattice up to a different depth in each sample. However, as illustrated by the normalized reflectance spectra in Figure 5B–D, the apparent color in a given region depends only on the number of unfilled layers ($N - n$) and is relatively insensitive to the total thickness (N).

While at face value this technique is far less simple and straightforward than the uniformly mixed functionalities described in the previous section, it possesses two important advantages with respect to the colorimetric differentiation of liquids: (i) the minimum colorimetrically discernible difference in wettability can be smaller for vertical gradients than for uniformly functionalized IOFs (for the same short-range variability in the neck angle, φ_0); and (ii) a single vertical gradient produces many distinct patterns in many different liquids. Vertical gradients allow enhancement of the colorimetric selectivity, not by decreasing the range of θ_c over which partial infiltration patterns are observed, but by transforming partial infiltration patterns to a form that become easy to mutually distinguish visibly (*i.e.*, have countable differences).

Figure 6A,B shows two percolation simulations (using the model described above with 15-layer IOFs) comparing IOFs with uniform and graded surface chemistry that illustrate this effect. Figure 6A shows the filling fraction as a function of the depth in an IOF ($\langle\varphi_0\rangle = 19.6°$, SD($\varphi_0$) = 3°) with spatially homogeneous surface chemistry for liquids with all integer θ_c values over the range [12–27°]. Figure 6B shows simulated infiltration profiles for the same IOF structure with θ_c increasing with depth. To approximate the type of gradation that might be produced by short oxygen plasma exposure, we let θ_c as a function of depth obey a cumulative normal distribution (mean = 7 layers, SD = 3 layers), having the same values as Figure 6A (shown for each curve in Figure 6B) at the top layer but

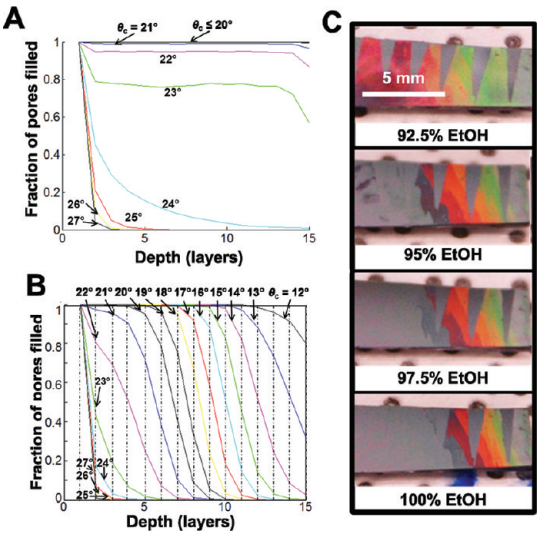

Figure 6. (A,B) Simulated layer-by-layer wetting profiles for liquids differentiated by one degree of intrinsic contact angle (12–27°), in an IOF ($\langle\varphi_0\rangle$ = 19.6°, SD(φ_0) = 3°) with spatially uniform wettability (A) and a graded wettability (B), where the intrinsic contact angle increases with depth by 10° (12–27° at layer 1, 22–37° at layer 15) according to a cumulative normal distribution (mean = 7 layers, SD = 3 layers). The boundary condition of a completely filled top layer (half-spheres) is assumed in all simulations. (C) Photographs illustrating the colorimetric distinction of different ethanol–water mixtures using an IOF functionalized with a vertical gradient DEC→13FS (45 s plasma exposure).

increasing with depth by a total magnitude of 10° over 15 layers (12–27° at layer 1, 22–37° at layer 15). As shown in Figure 6A, partial wetting in uniformly functionalized IOFs take on two qualitative forms. For θ_c higher than the percolation threshold ($\theta_c > 23°$ for this IOF), the filling fraction decays exponentially with depth. As argued previously, these filling profiles can be colorimetrically identified as unfilled because regions of sufficiently large total thickness will contain completely unfilled layers that produce bright color. For θ_c lower than the percolation threshold ($\theta_c \leq 23°$ in Figure 6A), the filling fraction is roughly homogeneous throughout the structure.

Since the iridescent color of IOFs, like most structurally colored materials, depends on the viewing angle, the comparison of colors in a nonbinary fashion (*e.g.*, using a color guide) could prove difficult. In contrast to uniformly functionalized IOFs, partial filling patterns produced by vertical chemical gradients are easy to distinguish by eye in our IOFs because they contain natural variations in total film thickness. What is notable about the curves in Figure 6B is that most (*e.g.*, θ_c = 13–21°) display the same filling profile, but successive curves are shifted by one or more layers. Recalling that, as shown in Figures 4 and 5, completely filled layers do not contribute to the color of an IOF, adjacent curves in Figure 6B would appear as identical "rainbow" patterns, shifted in space by one-layer step in an IOF having a varying total thickness such as in Figure 5A.

These patterns could be easily visually differentiable at any angle because, instead of comparing colors (each of which are viewing-angle-dependent), the problem has been reduced to that of measuring the distance (or counting the number of layer steps) to the start of the rainbow pattern.

Figure 6C shows a DEC→13FS (45 s etch time) vertical gradient in which 92.5% EtOH, 95% EtOH, 97.5% EtOH, and 100% EtOH are distinguished colorimetrically. In this sample, a 2.5% increase in ethanol concentration is sufficient to increase the final filling depth by enough to produce a clearly different visual pattern, thus improving by a factor of 2 the 5% selectivity achieved with the uniform mixtures described above. An array of hydrophilic "teeth" have been defined *via* selective oxidation[43] to aid in the visualization (*i.e.*, increase the countable nature of the readout).

Guiding the Eye. An important ingredient in the design of any colorimetric indicator is that it is as easy to read as possible. We can enhance the visual perceptibility of WICK readings by selectively oxidizing (to make lyophilic) certain regions of the IOFs as a last step to control the patterns that appear in the different liquids.[43] These lyophilic regions are being infiltrated by any liquid, thus providing an easy to read background pattern to guide the eye. Figure 7 shows four examples of indicator strips using both homogeneously mixed monolayers (Figure 7A) and vertical gradients of wettability (Figure 7B–D), where this extra step has been incorporated to enhance the readability of the strips.

Figure 7A,B shows indicators that mutually distinguish methanol (γ = 22.1 mN/m), ethanol (γ = 21.8 mN/m), and isopropyl alcohol (γ = 20.9 mN/m). The sample in Figure 7A consists of two chips, held together: on the left, the letter "M" has been defined (by oxidizing the background) in an IOF that is functionalized by the evaporation of a solution containing 1% 13FS-trichlorosilane (99% DEC); on the right, the letter "E" has been functionalized using 16.7% 13FS. When the two are submerged together, they read "ME" for methanol, "E" for ethanol, and appear blank in isopropyl alcohol. In Figure 7B, the same alcohols are distinguished in an IOF that has been functionalized with a DEC→13FS vertical gradient. In this sample, the IOF thickness increases from the left to the right, thus increased penetration depth of the liquids shifts the colored rainbow to the right. To enhance the readability of the patterns produced by vertical gradients, we patterned the functionalized region into an array of teeth by selectively oxidizing the background. This patterning reduces a "measuring" problem to a "counting" problem, which is easier to do roughly by eye (*i.e.*, without a ruler). Methanol, ethanol, and isopropyl alcohol are distinguished simply by counting the number of teeth visible. As each "tooth" contains only two- or three-layer steps, a change in penetration depth of ~1 layer (*e.g.*, ethanol *vs* isopropyl alcohol) induces the disappearance of a large fraction of the third tooth from the left. Figure 7C shows the same strategy applied to differentiating aliphatic compounds. Distinct teeth profiles are viewed in hexane (γ = 18.6 mN/m), heptane (γ = 19.9 mN/m), octane (γ = 21.4 mN/m), nonane (γ = 22.6 mN/m), and decane (γ = 23.6 mN/m).

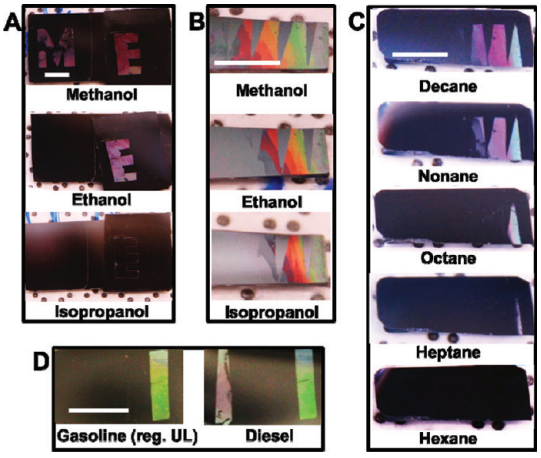

Figure 7. (A) Two IOFs, functionalized from evaporation of solutions containing 99:1 ("M") and 5:1 ("E") ratios of DEC- and 13FS-trichlorosilanes, are used to distinguish between alcohols. The backgrounds of the IOFs have been selectively oxidized to reveal "ME" in methanol, "E" in ethanol, and no color in isopropyl alcohol. (B,C) Photographs of IOFs functionalized with a vertical gradient of wettability (DEC→13FS) to distinguish between alcohols and alkanes. An array of teeth is oxidized (so that $\theta_c \rightarrow \sim 0$ in these regions for all liquids) to make the patterns easier to visibly distinguish. (D) Photographs of an IOF regionally functionalized with 13FS (right stripe) and a vertical gradient of DEC→13FS (left stripe) on an oxidized background that shows different patterns in samples of regular unleaded gasoline and diesel. Scale bars: 5 mm.

Figure 7D illustrates how regions of uniform functionality and vertical gradient can be combined in the same IOF. The IOF is patterned with two stripes on an oxidized (ROH)[43] background. The rightmost strip is functionalized with 13FS, while the leftmost stripe is composed of a vertical gradient of DEC→13FS. This is accomplished by masking the right half of the IOF during the short oxygen plasma step. The sample displays one stripe when immersed in regular unleaded gasoline and two stripes when immersed in diesel. These examples illustrate how a final oxidation step enhances the user-friendliness of WICKs. Through the use of a small legend sheet accompanying the chip, users could compare patterns or simply count the number of visible bars to quickly and reliably differentiate the set of liquids for which a given WICK has been optimized. These examples also illustrate how the design protocols developed in this paper for EtOH–water mixtures are generalizable to any list of liquids, from pure substances, to a complex mixture.

Applications and Limitations. In the above examples, we have demonstrated how WICK can be used to differentiate different, closely related liquids with remarkable selectivity (ethanol–water mixtures with varying concentrations, different pure alcohols and aliphatic compounds, and different grades of auto fuel). As WICK differentiates liquids based on their general property (wettability), this platform could be applied to any class of liquid. However, sensitive response to such a general property of liquids also means that chemical interference presents a significant challenge in WICK's application to chemical sensing. We envision that the WICK platform could be applied as an inexpensive and easy to use field test for (1) the authentication of liquid formulations (*e.g.*, for antiforgery or quality control) and (2) the identification of unknown liquids (*e.g.*, chemical spills, unlabeled containers, *etc.*). It is worth making the distinction between these two types of applications because of how the potential for chemical interference influences their applicability.

The key design characteristic that distinguishes liquid authentication from liquid identification is that the target liquid is known beforehand. In this case, it is possible, using the techniques presented in this paper, to design a strip that shows one pattern (*e.g.*, two stripes) in the target liquid but different patterns when the wettability is lowered (*e.g.*, three stripes) or raised (*e.g.*, one stripe) with respect to the target formulation. The fact that a change in the wetting properties of a liquid mixture can be induced by changes in any of the components of a given formulation is actually an advantage of WICK with respect to liquid quality authentication. An example of such an application would be to use WICK to protect against forgeries of a given grade of auto fuel.

Chemical interference is an important limitation to consider when applying WICKs for identification of unknown liquids. As with any sensor, which detects changes in a generic property of a substance (*e.g.*, density,[41,46] or pH in pH paper), it is not possible to deduce the specific chemical nature of an unknown without any prior information. However, it is rare that absolutely no information is given *a priori* about an unknown in practice. For example, an unlabeled beaker containing an unknown organic liquid in a lab that commonly uses a finite number of solvents (*e.g.*, acetone, isopropyl alcohol, hexane) most likely contains one of these. In this case, a WICK designed to have distinct responses only in these liquids would be sufficiently selective to identify the unknown. As is illustrated in several examples in this paper, this type of indicator could also be useful for rough determination of the relative concentrations of effectively two-component mixtures. Liquor would be an example of this type of mixture, where ethanol and water are the primary components, and the surface tension contrast of the two components is very high. In this case, we could expect interference to restrict the precision of ethanol concentration measurement somewhat, but not prohibitively. In contrast, it would not be able to give any information about the minor components (*e.g.*, sugars, *etc.*) unless there was extremely precise prior knowledge of the ethanol concentration.

The fundamental desirable characteristics of WICK as a field test for differentiating organic liquids are the simplicity of the readout and that the response is tied to a generic physical property that all liquids possess. While tests of similar simplicity can already be done for liquids with certain properties (*e.g.*, pH paper immersion for pH, ignition for flammability), this platform extends these capabilities to types of liquids that current techniques cannot access (*e.g.*, differentiating toxic, but nonflammable, chemicals). It is worth making brief comparison to a similar simple technique developed to differentiate organic liquids based on their density using magnetic levitation.[41,46] This technique shares many of the advantages that pertain to WICK (*e.g.*, sensitivity to a generic property of liquids) as well as the potential disadvantages (*e.g.*, chemical interference). One notable point of contrast, however, is simplicity—an instant colorimetric readout of countable patterns from a single solid-supported film is a level of simplicity that is difficult to improve upon. However, this does come at the cost of sensitivity in comparison to magnetic levitation.[46]

CONCLUSIONS

While colloidally templated inverse-opals have long been exploited for the manipulation of light,[5] we have shown here that, if such inverse-opals are produced with highly regular porosity and leveraged by simple protocols to adjust the surface chemistry, they can also be used to control the wetting of liquids with remarkable selectivity. The inherent coupling of the structure's fluidic and optical responses, easily controlled *via* the surface chemistry, lends this platform to broad applications. Two examples of such applications are a scheme for multilevel encryption[43] and the class of simple, portable colorimetric indicators for organic liquids detailed here.

We have shown that, through simple surface modifications using combinations of alkylchlorosilane chemistry and oxygen plasma, one can tailor the optofluidic response of an inverse-opal to differentiate closely related organic liquids over a broad range. With spatially selective oxidation to map a background pattern, this colorimetric response can be easily transformed into simple-to-read patterns. Using surface tension as the basis for identification, WICK exploits sensitivity to a generic property of all liquids. To illustrate this, we have shown indicators that differentiate pure substances (pure alcohols and alkanes), simple two-component mixtures (different ethanol

concentrations in water), and complex mixtures (gasoline and diesel). We foresee many applications of WICK, ranging from simple and inexpensive forgery detection to in-field liquid identification.

METHODS

IOF Synthesis. Large-area, crack-free inverse-opal films (IOFs) were fabricated according to the procedure detailed in refs 42 and 43.

Quality Control. After calcination, IOFs were cleaned in acid piranha solution for 4 h (85 °C). All were then exposed first to vapors of *n*-decyl (DEC) trichlorosilane for 24 h under vacuum, followed by baking at 150 °C for 20 min. Vapor-phase silanization is chosen to decouple the surface modification with the ability of liquid reagents to penetrate the porous network.[47] Baking steps under atmospheric pressure and ambient humidity were done after all silane exposures to ensure complete reaction of the chlorosilane moieties and cross-linking of adjacent surface-bound organosilanes.[47] To test for viability before use, wetting in the IOFs was first characterized with this DEC functionality in 85 and 90 vol % ethanol in water. In order to be considered for further use, an IOF had to display an unfilled state in 85% and a completely filled state in 90% (*e.g.*, see main text, Figure 2A). In samples that satisfied these requirements, the uniform DEC functionality was erased *via* O_2 plasma exposure for 1 h, followed by acid piranha cleaning (4 h, 85 °C), followed by a second hour of O_2 plasma exposure.

Deposition of Heterogeneous (Mixed) Functionalities. IOFs were exposed for 24 h to mixed 13FS (1*H*,1*H*,2*H*,2*H*-tridecafluorooctyl)- and DEC-trichlorosilane vapors by placing them under vacuum in a desiccator along with two small vials, each containing 200 μL of a 13FS- and DEC-trichlorosilane liquid−liquid mixture and a small dish containing dry desiccant (Drierite). The ratios shown in Figure 3B and Figure 7A represent the liquid volume ratios in these vials. Following silane exposure, IOFs were baked at 150 °C under atmospheric pressure and ambient humidity for 20 min.

Vertical Gradients of Wettability. IOFs were exposed under vacuum to vapors of 13FS-trichlorosilane for 24 h. After baking for 20 min at 150 °C under atmospheric pressure and ambient humidity, IOFs were exposed to O_2 plasma (5−10 sccm) for 10−120 s. All were then exposed to vapors DEC-trichlorosilane for 24 h under vacuum, followed by baking at 150 °C for 20 min under atmospheric pressure and ambient humidity.

Defining Hydrophilic Patterns (Guiding the Eye). To aid in visualization, hydrophilic regions were sometimes defined in IOFs using masked O_2 plasma exposure. Polydimethylsiloxane (PDMS) masks (2−5 mm thick) were prepared by pouring a 10:1 (wt) mixture of PDMS resin and cross-linking agent (Sylgard 184, Dow Corning) into a clean, empty tissue culture dish and curing for 24 h at 70 °C. Patterns were carved in freshly cured slabs with a scalpel or razor blade, and masks were discarded after one use. The PDMS masks (*e.g.*, letters) were held against the IOFs under roughly uniform pressure from a glass coverslip. The sample was exposed in this state to oxygen plasma for 10−30 min (5−10 sccm) to render the unmasked regions wetting to all liquids.

Acknowledgment. We thank T.L. Vu, A.V. Shneidman, L. Mishchenko, A.W. Rodriguez, B.D. Hatton, M. Aizenberg, and F. Spaepen for helpful discussions, and T.S. Wong for surface tension measurements. This work was supported by the AFOSR Award No. FA9550-09-1-0669-DOD35CAP. I.B.B. acknowledges support from the Natural Sciences and Engineering Research Council of Canada through the PGS-D program. M.K. acknowledges support from the Alexander von Humboldt Foundation. Electron microscopy was performed at Harvard's Center for Nanoscale Systems.

REFERENCES AND NOTES

1. Vukusic, P.; Sambles, J. R. Photonic Structures in Biology. *Nature* **2003**, *424*, 852–855.
2. Zheng, Y. M.; Gao, X. F; Jiang, L. Directional Adhesion of Superhydrophobic Butterfly Wings. *Soft Matter* **2007**, *3*, 178–182.
3. Sato, O.; Kubo, S.; Gu, Z. Z. Structural Color Films with Lotus Effects, Superhydrophilicity, and Tunable Stop-Bands. *Acc. Chem. Res.* **2009**, *42*, 1–10.
4. Fang, Y.; Sun, G.; Cong, Q.; Chen, G.-H.; Ren, L.-Q. Effects of Methanol on Wettability of the Non-smooth Surface on Butterfly Wing. *J. Bionic Eng.* **2008**, *5*, 127–133.
5. Aguirre, C. I.; Reguera, E.; Stein, A. Tunable Colors in Opals and Inverse Opal Photonic Crystals. *Adv. Funct. Mater.* **2010**, *20*, 2565–2578.
6. Schroden, R. C.; Al-Daous, M.; Blanford, C. F.; Stein, A. Optical Properties of Inverse Opal Photonic Crystals. *Chem. Mater.* **2002**, *14*, 3305–3315.
7. Arpin, K. A.; Mihi, A.; Johnson, H. T.; Baca, A. J.; Rogers, J. A.; Lewis, J. A.; Braun, P. V. Multidimensional Architectures for Functional Optical Devices. *Adv. Mater.* **2010**, *22*, 1084–1101.
8. Fendler, J. H.; Meldrum, F. C. The Colloid-Chemical Approach to Nanostructured Materials. *Adv. Mater.* **1995**, *7*, 607–632.
9. van Blaaderen, A.; Ruel, R.; Wiltzius, P. Template-Directed Colloidal Crystallization. *Nature* **1997**, *385*, 321–324.
10. Xia, Y. N.; Gates, B.; Yin, Y. D.; Lu, Y. Monodispersed Colloidal Spheres: Old Materials with New Applications. *Adv. Mater.* **2000**, *12*, 693–713.
11. Subramanian, G.; Manoharan, V. N.; Thorne, J. D.; Pine, D. J. Ordered Macroporous Materials by Colloidal Assembly: A Possible Route to Photonic Bandgap Materials. *Adv. Mater.* **1999**, *11*, 1261–1265.
12. Arsenault, A. C.; Clark, T. J.; von Freymann, G.; Cademartiri, L.; Sapienza, R.; Bertolotti, J.; Vekris, E.; Wong, S.; Kitaev, V.; Manners, I.; *et al.* From Colour Fingerprinting to the Control of Photoluminescence in Elastic Photonic Crystals. *Nat. Mater.* **2006**, *5*, 179–184.
13. Boriskina, S. V.; Lee, S. Y. K.; Amsden, J. J.; Omenetto, F. G.; Dal Negro, L. Formation of Colorimetric Fingerprints on Nano-Patterned Deterministic Aperiodic Surfaces. *Opt. Express* **2010**, *18*, 14568–14576.
14. Amsden, J. J.; Perry, H.; Boriskina, S. V; Gopinath, A.; Kaplan, D. L.; Dal Negro, L.; Omenetto, F. G. Spectral Analysis of Induced Color Change on Periodically Nanopatterned Silk Films. *Opt. Express* **2009**, *17*, 21271–21279.
15. Fudouzi, H.; Xia, Y. Photonic Papers and Inks: Color Writing with Colorless Materials. *Adv. Mater.* **2003**, *15*, 892–896.
16. Smay, J. E.; Cesarano, J., III; Lewis, J. A. Colloidal Inks for Directed Assembly of 3-D Periodic Structures. *Langmuir* **2002**, *18*, 5429–5437.
17. Kim, H.; Ge, J.; Kim, J.; Choi, S.; Lee, H.; Lee, H.; Park, W.; Yin, Y.; Kwon, S. Structural Colour Printing Using a Magnetically Tunable and Lithographically Fixable Photonic Crystal. *Nat. Photonics* **2009**, *3*, 534–540.
18. Brozell, A. M.; Muha, M. A.; Abed-Amoli, A.; Bricarello, D.; Parikh, A. N. Patterned When Wet: Environment-Dependent Multifunctional Patterns within Amphiphilic Colloidal Crystals. *Nano Lett.* **2007**, *7*, 3822–3826.
19. Potyrailo, R. A.; Ghiradella, H.; Vertiatchikh, A.; Dovidenko, K.; Cournoyer, J. R.; Olson, E. Morpho Butterfly Wing Scales Demonstrate Highly Selective Vapour Response. *Nat. Photonics* **2007**, *1*, 123–128.
20. Bonifacio, L. D.; Puzzo, D. P.; Breslav, S.; Wiley, B. M.; McGreer, A.; Ozin, G. A. Towards the Photonic Nose: A Novel Platform for Molecule and Bacteria Identification. *Adv. Mater.* **2010**, *22*, 1351–1354.
21. Albert, K. J.; Lewis, N. S.; Schauer, C. L.; Sotzing, G. A.; Stitzel, S. E.; Vaid, T. P.; Walt, D. R. Cross-Reactive Chemical Sensor Arrays. *Chem. Rev.* **2000**, *100*, 2595–2626.

22. Zhang, J. T.; Wang, L.; Luo, J.; Tikhonov, A.; Kornienko, N.; Asher, S. A. 2-D Array Photonic Crystal Sensing Motif. *J. Am. Chem. Soc.* **2011**, *133*, 9152–9155.
23. Lee, K.; Asher, S. A. Photonic Crystal Chemical Sensors: pH and Ionic Strength. *J. Am. Chem. Soc.* **2000**, *122*, 9534–9537.
24. Holtz, J. H.; Asher, S. A. Polymerized Colloidal Crystal Hydrogel Films as Intelligent Chemical Sensing Materials. *Nature* **1997**, *389*, 829–832.
25. Pursiainen, O. L. J.; Baumberg, J. J.; Ryan, K.; Bauer, J.; Winkler, H.; Viel, B.; Ruhl, T. Compact Strain-Sensitive Flexible Photonic Crystals for Sensors. *Appl. Phys. Lett.* **2005**, *87*, 101902.
26. Lee, Y. J.; Braun, P. V. Tunable Inverse Opal Hydrogel pH Sensors. *Adv. Mater.* **2003**, *15*, 7–8.
27. Pan, Z.; Ma, J.; Yan, J.; Zhou, M.; Gao, J. Response of Inverse-Opal Hydrogels to Alcohols. *J. Mater. Chem.* **2012**, DOI: 10.1039/c1jm13955j.
28. Endo, T.; Yanagida, Y.; Hatsuzawa, T. Colorimetric Detection of Volatile Organic Compounds Using a Colloidal Crystal-Based Chemical Sensor for Environmental Applications. *Sens. Actuators, B* **2007**, *125*, 589–595.
29. Lee, Y. J.; Pruzinsky, S. A.; Braun, P. V. Glucose-Sensitive Inverse Opal Hydrogels: Analysis of Optical Diffraction Response. *Langmuir* **2004**, *20*, 3096–3106.
30. Martinez, A. W.; Phillips, S. T.; Whitesides, G. M. Three-Dimensional Microfluidic Devices Fabricated in Layered Paper and Tape. *Proc. Natl. Acad. Sci. U.S.A.* **2008**, *105*, 19606–19611.
31. Clelland, C. T.; Risca, V.; Bancroft, C. Hiding Messages in DNA Microdots. *Nature* **1999**, *399*, 533–534.
32. Margulies, D.; Felder, C. E.; Melman, G.; Shanzer, A. A Molecular Keypad Lock: A Photochemical Device Capable of Authorizing Password Entries. *J. Am. Chem. Soc.* **2007**, *129*, 347–354.
33. Thomas, S. W.; Chiechi, R. C.; Lafratta, C. N.; Webb, M. R.; Lee, A.; Wiley, B. J.; Zakin, M. R.; Walt, D. R.; Whitesides, G. M. Infochemistry and Infouses for the Chemical Storage and Transmission of Coded Information. *Proc. Natl. Acad. Sci. U. S.A.* **2009**, *106*, 9147–9150.
34. Sagiv, J. Organized Monolayers by Adsorption. 1. Formation and Structure of Oleophobic Mixed Monolayers on Solid Surfaces. *J. Am. Chem. Soc.* **1980**, *102*, 92–98.
35. Lin, M.-H.; Chen, C.-F.; Shiu, H.-W.; Chen, C.-H.; Gwo, S. Multilength-Scale Chemical Patterning of Self-Assembled Monolayers by Spatially Controlled Plasma Exposure: Nanometer to Centimeter Range. *J. Am. Chem. Soc.* **2009**, *131*, 10984–10991.
36. Smith, R. K.; Lewis, P. A.; Weiss, P. S. Patterning Self-Assembled Monolayers. *Prog. Surf. Sci.* **2004**, *75*, 1–68.
37. Lercel, M. J.; Craighead, H. G.; Parikh, A. N.; Seshadri, K.; Allara, D. L. Sub-10nm Lithography with Self-Assembled Monolayers. *Appl. Phys. Lett.* **1996**, *68*, 1504–1506.
38. Piner, R. D.; Zhu, J.; Xu, F.; Hong, S. H.; Mirkin, C. A. "Dip-Pen" Nanolithography. *Science* **1999**, *283*, 661–663.
39. Lee, J.-T.; George, M. C.; Moore, J. S.; Braun, P. V. Multiphoton Writing of Three-Dimensional Fluidic Channels within a Porous Matrix. *J. Am. Chem. Soc.* **2009**, *131*, 11294–11295.
40. Rohr, T.; Hilder, E. F.; Donovan, J. J.; Svec, F.; Frechet, J. M. J. Photografting and the Control of Surface Chemistry in Three-Dimensional Porous Polymer Monoliths. *Macromolecules* **2003**, *36*, 1677–1684.
41. Mirica, K. A.; Phillips, S. T.; Shevkoplyas, S. S.; Whitesides, G. M. Using Magnetic Levitation To Distinguish Atomic-Level Differences in Chemical Composition of Polymers, and To Monitor Chemical Reactions on Solid Supports. *J. Am. Chem. Soc.* **2008**, *130*, 17678–17680.
42. Hatton, B. D.; Mishchenko, L.; Davis, S.; Sandhage, K. H.; Aizenberg, J. Assembly of Large-Area, Highly Ordered, Crack-Free Inverse Opals. *Proc. Natl. Acad. Sci. U.S.A.* **2010**, *107*, 10354–10359.
43. Burgess, I. B.; Mishchenko, L.; Hatton, B. D.; Kolle, M.; Lončar, M.; Aizenberg, J. Encoding Complex Wettability Patterns in Chemically Functionalized 3D Photonic Crystals. *J. Am. Chem. Soc.* **2011**, *133*, 12430–12432.
44. Tuteja, A.; Choi, W.; Mabry, J. M.; McKinley, G. H.; Cohen, R. E. Robust Omniphobic Surfaces. *Proc. Natl. Acad. Sci. U.S. A.* **2008**, *105*, 18200–18205.
45. Lorenz, C. D.; Ziff, R. M. Precise Determination of the Bond Percolation Thresholds and Finite-Size Scaling Corrections for the sc, fcc, and bcc Lattices. *Phys. Rev. E* **1998**, *57*, 230–236.
46. Mirica, K. A.; Shevkoplyas, S. S.; Phillips, S. T.; Gupta, M.; Whitesides, G. M. Measuring Densities of Solids and Liquids Using Magnetic Levitation: Fundamentals. *J. Am. Chem. Soc.* **2009**, *131*, 10049–10058.
47. Jung, G.-Y.; Li, Z.; Wu, W.; Chen, Y.; Olynick, D. L.; Wang, S.-Y.; Tong, W. M.; Williams, R. S. Vapor-Phase Self-Assembled Monolayer for Improved Mold Release in Nanoimprint Lithography. *Langmuir* **2005**, *21*, 1158–1161.